Coupled fluid flow and geomechanical deformation modeling

Susan E. Minkoff[a,*], C. Mike Stone[b,1], Steve Bryant[c,2],
Malgorzata Peszynska[c,2], Mary F. Wheeler[c,2]

[a]*Department of Mathematics and Statistics, University of Maryland, Baltimore County, 1000 Hilltop Circle, Baltimore, MD 21250, USA*
[b]*Computational Solid Mechanics and Structural Dynamics Department 9142, Mail Stop 0847, Sandia National Laboratories,
Albuquerque, NM 87185, USA*
[c]*Center for Subsurface Modeling, Texas Institute for Computational and Applied Mathematics (TICAM), The University of Texas at Austin,
Austin, TX 78712, USA*

Abstract

Accurate prediction of reservoir production in structurally weak geologic areas requires both mechanical deformation and fluid flow modeling. Loose staggered-in-time coupling of two independent flow and mechanics simulators captures much of the complex physics at a substantially reduced cost. Two 3-D finite element simulators—Integrated Parallel Accurate Reservoir Simulator (IPARS) for flow and JAS3D for mechanics—together model multiphase fluid flow in reservoir rocks undergoing deformation ranging from linear elasticity to large, nonlinear inelastic compaction. The loose coupling algorithm uses a high-level driver to call the flow simulator for a set of time steps with fixed reservoir properties. Pore pressures from flow are used as loads for the geomechanics code in the determination of stresses, strains, and displacements. The mechanics-derived strain is used to calculate changes to the reservoir parameters (porosity and permeability) for the next set of flow time steps. Mass is conserved in the coupled code despite dynamically changing reservoir parameters via a modification to the Newton system for the flow equations, and an approximate rock compressibility becomes a useful preconditioner to help with convergence of the modified flow equations. Two numerical experiments illustrate the accuracy of the coupled code. The first example is a quarter-five-spot waterflood undergoing poroelastic deformation, which is validated against a fully coupled simulator. Vertical displacements at the well locations match to within 10%. Moreover, experimentation shows that 13 mechanics time steps (taken over the course of 5 years of simulation time) were sufficient to achieve this result (a substantial cost savings over full coupling in which both the mechanics and flow equations must be solved at each time step). The second numerical example is based on real data from the Belridge Field in California, which illustrates one of the complex plastic constitutive relationships available in the coupled code. The results mimic behavior which was observed in the field. The coupled code serves as a prototype for loosely coupling together any two preexisting simulators modeling diverse physics. This technique produces a coupled code relatively quickly and inexpensively and has the advantage of accurately modeling complex nonlinear phenomena often

* Corresponding author. Tel.: +1-410-455-3029; fax: +1-410-455-1066.
E-mail addresses: sminkoff@math.umbc.edu (S.E. Minkoff), cmstone@sandia.gov (C.M. Stone), sbryant@ticam.utexas.edu (S. Bryant), mpesz@ticam.utexas.edu (M. Peszynska), mfw@ticam.utexas.edu (M.F. Wheeler).
[1] Fax: +1-505-844-9297.
[2] Fax: +1-512-232-2445.

observed in a real field but difficult to capture with a fully coupled simulator. Further, the code has produced promising results when used for time-lapse studies of compactible reservoirs.

1. Introduction

To understand the response of reservoirs located in structurally weak geologic formations, engineers must use coupled flow simulation and mechanical deformation modeling. While the majority of reservoirs are located in stable rock formations that do not undergo deformation, there are many reasons to investigate coupled flow and geomechanics. Even over-pressurized reservoirs located in stable environments may undergo ''settling'' at the start of production. Coupled flow and mechanics are necessary for predicting well failures and guiding well placement and production. Modeling of offshore reservoirs near salt bodies can also be modeled effectively in this way.

There are three basic algorithms for multiphysics simulation: full coupling, loose coupling, and one-way coupling. To define a fully coupled simulator, a single set of equations (generally a large system of nonlinear coupled partial differential equations) incorporating all of the relevant physics must be derived. As an example, the traditional porous flow equations for a rigid matrix would be modified to include terms for mechanical deformation. Full coupling is often the preferred method for simulating multiple types of physics simultaneously since it should theoretically produce the most realistic results. Unfortunately, deriving a fully coupled multiphase flow simulator that models nonlinear, inelastic mechanical deformation is extremely difficult. Thus with fully coupled models, one generally simplifies to single-phase flow and even more commonly, simplifies the mechanics to linear elasticity (Lewis and Sukirman, 1993a,b; Lewis and Ghafouri, 1997; Osorio et al., 1999).

At the other end of the spectrum is one-way coupling in which two essentially separate sets of equations are solved independently over the same total time interval. Periodically, output from one simulator is passed as input to the other; however, information is passed in only one direction. For example, pore pressures might be sent from the flow code to load the mechanics calculation of stresses, strains, and displacements. No information would be passed back from mechanics to flow, however. In most practical applications, the two simulators are in fact run independently. One can often gain valuable insight into the physical situation from one-way coupling, and it is clearly preferable (in situations where mechanics is important) to fluid flow alone. A very successful one-way coupling experiment was performed to predict well failures in the Belridge Field, California. This work included a 200-well fluid flow simulation intended to help with prediction of well failure rates in other parts of the field (Fredrich et al., 1996, 1998).

The present work describes a ''loose coupling'' algorithm situated somewhere between full and one-way coupling. In loose coupling, there are two sets of equations which are solved independently (as in one-way coupling), but information is passed at designated time intervals in both directions between the two simulators (fluid flow and geomechanics). Loose coupling has the advantage of being relatively simple to implement (like one-way coupling), but it holds promise for capturing much more of the complex nonlinear physics, and thus is closer to a fully coupled approach. Loose coupling capitalizes on decades of algorithm and code development in different application domains while yielding a coupled model in much less time than would be required to create a fully coupled model. Two independently developed simulators were coupled together: fluid flow from the University of Texas at Austin (IPARS) and mechanics from Sandia National Labs (JAS3D). IPARS can map faults and contains multiple physical flow models that can run in different parts of the reservoir domain in a single simulation. JAS3D can handle large, nonlinear inelastic deformation and sliding contact surfaces (as well as numerous other types of mechanics).

The loose coupling algorithm is similar in spirit to the methods described in the papers of Fung et al. (1994), Settari and Mourits (1994), and Settari and Walters (1999). One of the fundamental questions in loose coupling is how to best handle large jumps in flow simulation parameters coming from infrequent calls to mechanics (relative to the total number of flow/ mechanics time steps used in a fully coupled approach). Modifications to the flow equations can be made which allow dynamic changes to flow parameters while still maintaining conservation of mass. The paper begins with a description of the two simulators and an explanation of how each simulator was modified to allow incorporation of parameter updates from the other simulator. Two numerical experiments illustrate the accuracy and efficiency of the loose coupling scheme. The first experiment is a waterflood validation of the coupled code against a fully coupled poroelastic simulator. The loosely coupled simulator is run multiple times using a range of different mechanics time steps and the results are compared to the fully coupled simulator output. This experiment demonstrates that loose coupling can capture much of the physics of full coupling at considerably less cost. The second numerical example is based on data from the Belridge Field

in California—a field that underwent considerable nonrecoverable plastic deformation.

2. Loose coupling vs. other algorithms

The loose coupling algorithm is shown as a flow chart in Fig. 1. A high-level interface loosely couples these two simulators by invoking one simulator and then the other repeatedly over the total simulation time. The user designates a time step for switching from flow to mechanics (Δt_1, where $\Delta t_1 = t_1 - t_0$; a typical value of Δt being anywhere from 1 month to 1 year). The flow simulator runs for the designated time interval Δt_1 and will most likely break the Δt_1 time interval into multiple time steps. At the end of the time interval Δt_1, the pore pressure is passed to the mechanics code, and the mechanics code then runs the simulation for that same (prior) Δt_1 time interval. The geomechanics code may take only one time step for this time interval (or at least different sub-time steps relative to the flow simulator). The pore pressures used as loads allow the mechanics code to calculate strains and ultimately updates to porosity and permeability for the flow simulator's subsequent
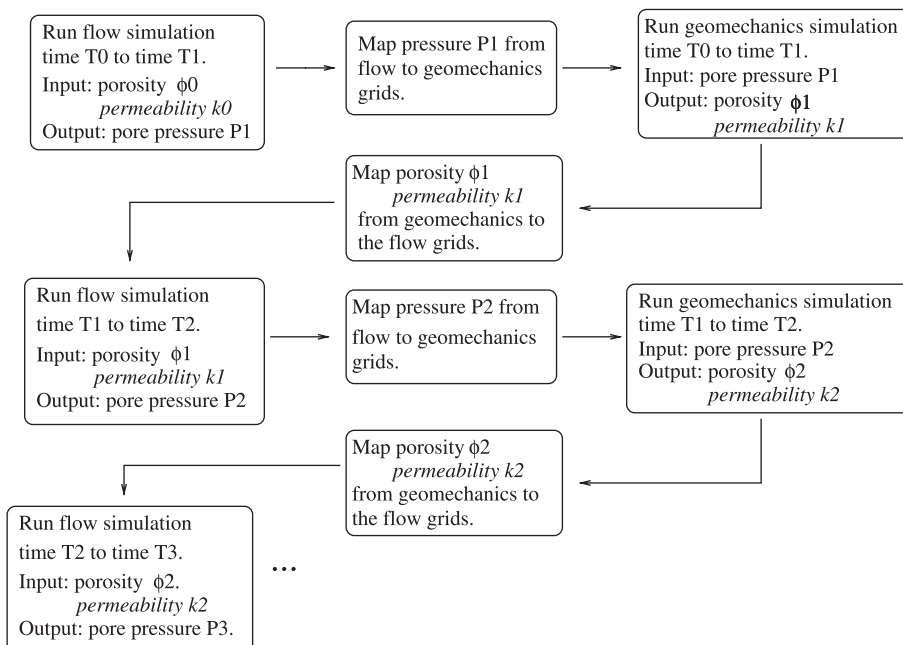

Fig. 1. Flow chart for loose coupling algorithm.

time steps. (For details on the calculation of updated flow parameters, refer to Sections 4 and 5.) Using the updated values of flow parameters from mechanics (time step Δt_1), fluid flow is simulated for the next time interval $\Delta t_2 = t_2 - t_1$. The two-way staggered-in-time coupling algorithm proceeds until both simulators reach the final time t_{end}.

Between the flow and mechanics simulations in Fig. 1, there is a column devoted to mapping output and input quantities from one simulator to the other. This column is necessary because the loose coupling algorithm does not require the two simulators to use the same computational grid. In fact, one of the advantages of loose coupling is that mechanics and flow need not have identical spatial grids. The flow domain is typically a subset of the mechanics domain. The flow simulator should only model the reservoir, while the mechanics code may need to extend further in the lateral directions than the reservoir, will surely need to extend up to the earth's surface (for over-burden loading), and may cover an area below the reservoir as well. Note that fully coupled simulators typically assume a single computational domain, so fluid flow is simulated outside of the reservoir (an unnecessary calculation). The current algorithm does not even require the two codes to have the same grid spacing in the parts of the domain where there is overlap (the reservoir). Physically, there may be a sound reason why the spatial discretization on the flow side will differ from that for mechanics (examples: multiple material layers in the reservoir or a need for finer resolution to capture complex physics).

Many upscaling and downscaling (or "averaging") tools are available for mapping quantities from one grid to another. The loose coupling simulator uses a software package from Sandia's engineering suite, Mapvar (Wellman, 1999). Mapvar provides a few different methods for accomplishing this mapping, and the coupled simulator invokes the most robust method for capturing gradients in the solution: variable values at element centers are scattered to the nodes via a linear constrained least squares fitting procedure. For a small sample of the upscaling literature, refer to Arbogast et al. (1998b), Hou and Wu (1997), E (1992), Durlofsky (1991), Durlofsky et al. (1994, 1996), Christie (1996), Christie et al. (1995), King et al. (1993, 1995), and Espedal and Saevareid (1994).

3. Description of simulators

3.1. Reservoir simulator

The fluid flow simulator, Integrated Parallel Accurate Reservoir Simulator (IPARS) (Wang et al., 1997; Parashar et al., 1997; Wheeler et al., 1999), developed at the University of Texas, is a three-dimensional general subsurface simulator that can be run serially or in parallel using MPI. It currently includes multiple physical models: single phase, two-phase oil–water and air–water, and a reactive transport, compositional model as well as the black oil model described below. IPARS contains several numerical discretizations of these physical models including mixed finite elements and discontinuous Galerkin finite elements for two-phase flow. The mixed finite element method gives a stencil equivalent to cell-centered finite differences if lowest order Raviart–Thomas spaces are used for approximation and the computational domain is rectangular (Russell and Wheeler, 1983; Arbogast et al., 1996, 1997). The scheme allows for discontinuity and for degeneracy of fluid–rock properties, and it has optimal convergence properties (Arbogast et al. 1996, 1997, 1998a). Additionally, different time discretizations have been implemented in IPARS including implicit, semi-implicit, and sequential.

The IPARS simulator was chosen for this work because of its unusual capabilities which are well suited to coupled flow and mechanics. One such feature allows the user to break the physical domain into subdomains corresponding to geologic blocks and then to apply different gridding or even different physical or numerical flow models to each block. As an example, certain production scenarios might best be understood via flow simulation which uses a compositional model. However, a black oil model might suffice for the parts of the reservoir domain far from the production wells. A version of domain decomposition mortar space-based methodology, originally formulated for single-phase flow (Arbogast et al., 1996; Yotov, 1998), was developed to ensure convergence across interfaces between these different subdomain blocks and models (Peszynska et al., 1999, 2002; Wheeler et al., 2000; Lu et al., 2001). IPARS' unique capacity to follow geologic structure (especially faults) via blocking makes it a good

choice for a sophisticated flow and mechanics simulator.

Although the IPARS framework makes it relatively easy to port code changes between different flow models, in this work the black oil model is used exclusively. Black oil is the simplest model which includes all three fluid phases (oil, gas, and water) needed for seismic time-lapse studies (Minkoff et al., 1999). In this black oil model, the reservoir is assumed to be isothermal, the permeability tensor is diagonal, and the viscosity of each phase is constant. No chemical reactions, precipitation, or adsorption are present, and the formation is slightly compressible. The external boundary conditions are no-flow Neumann conditions. Numerically, the black oil model code is fully implicit, 3-D, and uses an expanded mixed finite element method to maintain local conservation of mass (Lu, 2000; Lu et al., 2001).

3.1.1. Black oil formulation

Assume that two or three phases and three components are present. The uppercase subscripts W, O, and G are used for the fluid components: water, heavy hydrocarbon or oil, and light hydrocarbon or gas, respectively. Lowercase subscripts w, o, and g are used for the fluid phases: aqueous, oleic, and gaseous phase, respectively. The model is partially miscible. In particular, the water component exists only in the water phase and it is the only component in that phase. The gas phase contains only the gas component and may be absent if the pressure is high enough, and the oil phase may contain both the oil and gas components. The oil component is the residual liquid at atmospheric pressure after differential vaporization, while the gas component is the remaining fluid (Peaceman, 1977; Lake, 1989).

Given that N_I is the stock tank volume of component I ($I = $ O,G,W) per unit pore volume, ϕ is porosity, R_o is the stock tank volume of gas dissolved in a stock tank volume of oil, and q_I is the total stock tank rate of injection of component I, the mass balance equations are

$$\frac{\partial}{\partial t}(\phi N_G) = -\nabla \cdot (U_g + R_o U_o) + q_G$$

$$\frac{\partial}{\partial t}(\phi N_I) = -\nabla \cdot U_i + q_I \qquad I = \text{oil, water} \qquad (1)$$

Darcy's Law gives the mass velocity U of phase i (here $i = $ oil, gas, or water):

$$U_i = -\frac{Kk_{ri}}{B_i\mu_i} \cdot (\nabla P_i - \rho_i g \nabla D) \qquad (2)$$

Here, K is the absolute permeability tensor, and k_{ri} is the relative permeability of phase i. B_i is the formation volume factor for phase i. P_i is pressure, μ_i is viscosity, and ρ_i is density. Gravity has magnitude g, and D is depth. Finally, the saturations must satisfy the constraint:

$$S_g + S_o + S_w = 1$$

and capillary pressures are defined by

$$P_{cow}(S_w) = P_o - P_w$$

$$P_{cgo}(S_g) = P_g - P_o$$

The gas component is soluble in the oil phase. The maximum concentration of gas that can be dissolved in the oil phase at a given pressure is given by R_s. The subscript s stands for "saturated" conditions, and R_s is an increasing function of pressure. If the amount of gas contained in some element of volume is less than this maximum ($R_o < R_s$), then all the gas dissolves into the oil phase, so that $S_g = 0$. If the amount of gas in the element exceeds this maximum, then $R_o = R_s$, and a free gas phase exists, so that $S_g > 0$. Reducing the pressure of a volume of gas-saturated oil causes gas to come out of solution and form a free gas phase. Thus two-phase and three-phase conditions may prevail simultaneously in different regions of the same reservoir.

The state equations complete the formulation. Denote the stock tank density of component I by ρ_{IS}. Then, the water density is given by $\rho_w = \rho_{WS}/B_w$ and the density of the gas phase (if it exists) is given by $\rho_g = \rho_{GS}/B_g$. Both the equations $S_w = B_w N_W$ and $S_w = 1 - S_o - S_g$ define the water phase saturation. The oil phase density and saturation are related by $S_o = B_o N_O$ and $\rho_o = (\rho_{OS} + R_o\rho_{GS})/B_o$. Finally, gas saturation in three-phase conditions is $S_g = B_g(N_G - R_s N_O)$.

3.2. Geomechanical deformation modeling

The geomechanics code from Sandia National Laboratories, JAS3D, is a three-dimensional, quasi-

static finite element code. Like IPARS for fluid flow, JAS3D is a mechanical deformation code with several unique capabilities. Specifically, JAS3D can accurately model large deformations, sliding contact surfaces, and both elastic and inelastic material responses from a wide array of constitutive models (Arguello et al., 1998). The advanced finite element technology which is used in JAS3D is based on iterative quasistatic solvers which allow problems with large numbers of unknowns to be efficiently solved.

3.2.1. Traditional vs. explicit finite element approach

Consider the following field equation governing the deformation of a body occupying a volume, V,

$$\partial \sigma_{ij}/\partial x_j + \rho f_i = 0 \text{ on } V. \tag{3}$$

Eq. (3) is the quasi-static equation of motion, where σ_{ij} is the Cauchy stress tensor, x_j is the position vector, ρ is the mass per unit volume, and f_i is a specific body force vector. The solution to Eq. (3) is sought subject to the kinematic and traction boundary conditions

$$\theta_i(\boldsymbol{x}, t) = \Theta_i(\boldsymbol{x}, t) \text{ on } \Omega_{\mathrm{U}} \tag{4}$$

$$\sigma_{ij}\boldsymbol{n}_j = s_i(\boldsymbol{x}, t) \text{ on } \Omega_{\mathrm{T}} \tag{5}$$

where Ω_{U} represents the portion of the boundary on which kinematic quantities are specified (i.e., displacements, θ_i), $\boldsymbol{n}_j$ is a unit normal vector, and Ω_{T} represents the portion of the boundary on which tractions are specified. The boundary of the body is given by the union of Ω_{U} and Ω_{T}.

For the displacement-based finite element method, the equations described in the foregoing paragraph can be discretized and rewritten in one of two ways:

$$\left\{ \sum_N \int_{\mathrm{ve}} \mathbf{B}\boldsymbol{\sigma} \mathrm{d}V \right\} = \{\boldsymbol{F}\} \tag{6}$$

and

$$[\mathbf{K}(\theta)]\{\theta\} = \{\boldsymbol{F}\}, \tag{7}$$

where the term on the left-hand side of Eqs. (6) and (7) is the internal force vector, and $\{\boldsymbol{F}\}$ is the external force vector. In Eq. (6), $\mathbf{B}$ is the strain-displacement

transformation matrix, N is the number of elements in the finite element method (FEM) discretization, $\boldsymbol{\sigma}$ is an ordered vector of stress components in each element at a Gauss point, and ve is the volume of each element. In Eq. (7), $[\mathbf{K}(\theta)]$ represents the global stiffness matrix and $\{\theta\}$ represents the global vector of unknown nodal displacements. Both Eqs. (6) and (7) are included to highlight the difference in approach between the traditional FEM approach and the local-iterative approach used in this work.

The traditional FEM approach involves the direct solution of Eq. (7). Namely, an element stiffness and external force vector are formed for each element in the overall structure. The contributions from each of these element stiffness matrices and force vectors are then assembled into a global stiffness matrix and force vector describing the overall system. For the inelastic and/or geometrically nonlinear case (the stiffness matrix varies with the unknowns), the load is typically applied incrementally. The resulting nonlinear equations are then solved at each load increment with some variant of the Newton–Raphson method. The direct factorization of this sparse global stiffness matrix can result in (1) extremely large storage requirements and (2) a very large number of arithmetic operations, especially for three-dimensional problems. Commercially available software is generally limited and will typically only handle models on the order of tens of thousands of elements in size. When attempting to solve large problems of interest to the oil and gas industry, models on the order of hundreds of thousands to millions of elements may be needed. For problems of this size, the traditional direct solution approach becomes prohibitive due to memory and computational time requirements.

The iterative technology that is used in JAS3D never requires the formation of a global stiffness matrix. Instead, the divergence of the stress is found at the element level. Contributions to each node in the overall structure are summed (i.e., the vector described by the left side of Eq. (6)). A residual force vector made from the internal minus the external forces,

$$\{\boldsymbol{R}\} = \left\{ \sum_N \int_{\mathrm{ve}} \mathbf{B}\boldsymbol{\sigma} \mathrm{d}V \right\} - \{\boldsymbol{F}\}, \tag{8}$$

is computed, and the solution procedure is then one of reducing the residual to zero using an iterative techni-

que. Because the quantities being manipulated are vectors, there is no need to store or factor a global stiffness matrix. Consequently, the storage requirements are small when compared to the traditional FEM approach. Two iterative techniques are currently used in JAS3D—a preconditioned conjugate gradient technique (Biffle, 1993) and an adaptive dynamic relaxation technique (Stone, 1997). These two iterative techniques are both able to handle the nonlinearities associated with inelastic material response and sliding contact surfaces. Comparing performance of a commercially available FEM program against JAS3D on an inelastic problem with 250,000 elements, the traditional FEM code took 30 times more CPU time than was required to solve the same problem using JAS3D.

4. Modifications to fluid flow

Traditional flow simulators initialize porosity and permeability at the start of the computation and then these quantities remain fixed throughout the simulation. For coupled flow and mechanics, these quantities must be updated each time the code completes a JAS3D step.

4.1. Porosity updates

In traditional flow simulators, small changes to reservoir rock properties (porosity ϕ) are accounted for by the following linear expression:

$$\phi = \phi^*(1 + c_r(P - P^*)) \qquad (9)$$

where ϕ^* is the initial porosity at initial pressure P^*, and rock compressibility c_r is a constant (typically on the order of 10^{-7}–10^{-10} Pa^{-1}). The code uses water pressure, P_w, in place of pore pressure since water is the phase wetting the rock and thus a reasonable choice. A saturation-weighted average of the three fluid phase pressures also could be used. In reality, conventional black oil simulators assume that the reservoir geology (porosity and permeability) is changing very little (if at all) during flow simulation. In the coupled simulations, Eq. (9) is not used to determine porosity (although it is used for preconditioning the solver, as described below). Porosity values at the beginning of each set of simulation time

steps are input to the flow simulator from the mechanics portion of the code, as depicted in Fig. 1.

The nonlinear system resulting from the finite element discretization of Eqs. (1) and (2) is solved via Newton's method. Writing this system in matrix form gives $\mathbf{J}\mathbf{x} = -\mathbf{R}$, with $\mathbf{J}$ the Jacobian matrix of partial derivatives with respect to the primary variables $\mathbf{x} = [P_w, N_O, N_G]$, and R the residual. The solution vector $\mathbf{x}$ actually contains incremental changes in the primary variables.

Recalling a representative equation from the mass balance system for component α, the residual is

$$R_\alpha = \phi(N_\alpha^{n+1} - N_\alpha^n) + \mathrm{d}t(\nabla \cdot U_\alpha^{n+1} - q_\alpha^{n+1}) \qquad (10)$$

with the backward Euler method used for the time discretization. For coupled geomechanics and reservoir simulation, porosity updates at time step $n+1$ are introduced through the residual modification

$$R_\alpha = (\phi N_\alpha)^{n+1} - (\phi N_\alpha)^n + \mathrm{d}t(\nabla \cdot U_\alpha^{n+1} - q_\alpha^{n+1}). \qquad (11)$$

In other words, the porosity values at time step $n+1$ are provided by the mechanics code and directly incorporated into the Newton system to be solved. In the above formulation, mass is conserved, and the Newton update accounts for a decrease in pore space (for example) by increasing the well rates and pressures at the next time step.

4.2. Permeability updates

Dynamic updates of absolute permeability during flow simulation impact large portions of the code. The grid block transmissibilities in the discretized equations and parts of the well model must be continuously updated.

Rewriting Eq. (11) slightly, the water phase equation becomes:

$$\frac{(\phi N_W)^{n+1} - (\phi N_W)^n}{\Delta t^{n+1}} + \nabla \cdot U_W^{n+1} = q_W^{n+1} \qquad (12)$$

The oil and gas phase equations are similar. In the equation above, $\Delta t^{n+1} = t^{n+1} - t^n$. The correspond-

ing nonlinear residual equation used in Newton's method is

$$R_{\text{w},ijk}^K = V_{ijk}\{(\phi N_\text{w})_{ijk}^K - (\phi N_\text{w})_{ijk}^n + \Delta t^{n+1}$$
$$\times [\nabla \cdot U_\text{w} - q_\text{w}]_{ijk}^K\}. \tag{13}$$

The subscript ijk refers to the grid cell indexed by i in the x direction, j in the y direction, and k in the z direction. The superscript K refers to the Kth approximation to the superscripted quantity at time level $n+1$. The volume of grid cell ijk is denoted V_{ijk}.

From Darcy's Law (Eq. (2)), the component mass velocities in the residual equation above are discretized using cell-centered differencing in space,

$$\Delta t^{n+1} V_{ijk}(\nabla \cdot U_\text{w})_{ijk}^K = -\lambda_{\text{w},i+1/2,jk}^K\Big[P_{\text{w},i+1,jk}^K - P_{\text{w},ijk}^K$$
$$- \rho_{\text{w},i+1/2,jk}^K g(D_{i+1,jk} - D_{ijk})\Big]$$
$$+ \lambda_{\text{w},i-1/2,jk}^K\Big[P_{\text{w},ijk}^K - P_{\text{w},i-1,jk}^K$$
$$- \rho_{\text{w},i-1/2,jk}^K g(D_{ijk} - D_{i-1,jk})\Big]$$
$$+ \text{ similar terms for the } y \text{ and}$$
$$z \text{ directions.}$$

If K_{xx}, K_{yy}, and K_{zz} are harmonically averaged values of the absolute permeability tensor between adjacent grid cells, and Δx_i, Δy_j, and Δz_k are the edge lengths of a rectangular grid cell ijk, then the transmissibility constants that appear in the upstream-weighted mobility computation for λ are:

$$\lambda_{\text{w},i+1/2,jk}^K = \Delta t^{n+1} 2\Delta y_j \Delta z_k \left(\frac{\Delta x_i}{K_{xx,ijk}} + \frac{\Delta x_{i+1}}{K_{xx,i+1,jk}}\right)^{-1}$$
$$\times \left(\frac{k_\text{rw}}{B_\text{w}\mu_\text{w}}\right)_{sjk}^K$$

where $s=i$ if $P_{\text{w},ijk}^K \geq P_{\text{w},i+1,jk}^K$, and $s=i+1$ if $P_{\text{w},ijk}^K < P_{\text{w},i+1,jk}^K$. Upstream weighting is used similarly in the y and z directions.

The values of transmissibility are generally assumed fixed in uncoupled flow simulators. Here, they must be updated after each mechanics step to account for the permeability changes induced by strain. In the coupled code, permeability also must change dynamically in the well model. IPARS currently allows for two types of wells: bottom-hole pressure specified and

rate specified (Peaceman, 1983; Lu, 2000). The volumetric rate of flow of fluid phase i (i = w,o,g) from the well bore to a grid cell can be expressed as

$$Q_i = \frac{GLKk_\text{ri}}{\mu_i}(P_\text{wb} - P_i) \tag{14}$$

where P_wb is the well-bore pressure (hydrostatic pressure), P_i is the pressure of phase i in the grid cell, K is the absolute permeability of the grid cell, L is the length of the open well bore penetrating the grid cell, and G is a dimensionless geometric factor related to the well-bore radius and given by the Peaceman (1983) correction.

5. Modifications to mechanics

5.1. Porosity updates

The mechanics code is capable of calculating pointwise changes in pore volume in the reservoir, coming (for example) from field production, pressure decrease, and then compaction. To calculate these field property changes in the coupled code, the reservoir simulator sends the pore pressure field to the geomechanics part of the code where it is used in the calculation of total stress:

$$\sigma_{ij}^\text{T} = \sigma_{ij} + p\delta_{ij}.$$

Here p is the pore fluid pressure, δ_{ij} is the Kronecker delta function, and σ_{ij} is the "effective" stress which is used in the constitutive model. The total stress is used in the determination of the equilibrium state for the reservoir subject to the overburden loads, kinematic boundary conditions, and changing pore pressure field. On output, the geomechanics code provides an updated porosity, ϕ, at the current time step via the following expression:

$$\phi = 1 - \frac{(1 - \phi_0)}{e^{\epsilon_\text{v}}}$$

where ϕ_0 is the initial porosity, and ϵ_v is the total volume strain (the sum of the elastic and inelastic components of strain). JAS3D uses a description for the motion of the continuum that is valid for the large deformation response of the reservoir rock.

5.2. Permeability updates

Using available permeability-differential stress data for several different rock types, a correlation can be established between permeability and total volume strain. The volume strain captures the pre-failure permeability decline as well as the large post-failure permeability reduction. After experimenting with several different functional forms relating permeability to volume strain, an exponential model that gave the best data fit was chosen:

$$K = A e^{B_{\epsilon_v}}.$$

Here A and B are material constants and ϵ_v is again the total volume strain. Because additional experimental data to define an anisotropic permeability tensor is not available, the change in the permeability expression is assumed to be isotropic. Given the requisite measured data, however, any other functional form for permeability could be substituted into the code.

6. Convergence issues—a Newton's method preconditioner for the coupled code

Although loose coupling enables modeling of realistic physics much more cheaply than full coupling (fewer mechanics time steps must be taken), this time savings is not for free. When the reservoir parameters change dynamically with time, the flow equations become more difficult to solve. After each JAS3D step, IPARS receives new values of permeability and porosity which are used for the next set of flow time steps. If mechanical deformation is linear elastic and the rock compressibility relationship relating porosity to pressure described by Eq. (9) holds, then the flow solver will have little difficulty searching for the next solution to the Newton system. By differentiating Eq. (9) with respect to pressure, changes in pore volume are estimated. This expression guides the flow solver towards a solution for the next time step. In the coupled code, mechanical deformation is not restricted to be linear elastic. JAS3D has a range of over 50 constitutive relationships for modeling deformation (Appendix A). This flexibility in material modeling, however, requires IPARS to grapple with incorporating a set of numbers

(representing updated reservoir parameters) without any information about the way in which the flow problem has changed. This lack of information can cause the IPARS solver to have difficulty converging.

To improve the convergence of the flow solver in the coupled code, the rock compressibility expression is reintroduced solely for the purpose of preconditioning the flow equations in IPARS. In other words, the user provides an approximate value for compressibility which is used to determine the derivative of Eq. (9) with respect to pressure. This derivative is used in forming the Jacobian for the Newton system. The actual values of reservoir porosity used in the flow equations still come entirely from the JAS3D computations, however. This strategy greatly improves IPARS' chances of converging after JAS3D time steps in which the reservoir properties change substantially with time.

7. Numerical examples

7.1. Validation experiment

The first numerical example in this paper is a validation experiment in which output from IPARS/JAS3D is compared to the solution from a fully coupled ARCO simulator, ACRES (Dean et al., 2003). ACRES uses finite differences to discretize the multiphase flow problem and finite elements for the mechanics calculation (displacements). The poroelastic equations are formulated in terms of total stresses, bulk strains, and fluid pressures. The nonlinear flow equations and linear poroelastic equations are fully coupled and solved iteratively using a Newton–Raphson technique. The Newton–Raphson method linearizes the equations which are then passed to a linear solver. The resulting matrix system is solved for block pressures, well pressures, and displacements.

The validation experiment is based on a waterflood with the domain containing one production well and one injection well—each of which is located in an opposite corner of the grid (a "quarter-five-spot pattern"). The waterflood simulation covers 25 years with a specified water injection rate of 79.5 m³/day and production rate for liquids of 119 m³/day. The production well is also assigned a limit of 3.45 MPa

(below which the bottom-hole pressure cannot fall). The average reservoir pressure will decline during simulation (producing compaction in the field) as the production rate is greater than the injection rate.

In this example, mechanical deformation is restricted to be elastic with reservoir compressibility of 1.1603×10^{-8} Pa^{-1}. (The pore compressibility is about the same magnitude as the total fluid compressibility in this case.) Poisson's ratio is set at 0.3, and Biot's constants α and M^{-1} have values of 1 and 0, respectively. The reservoir's top surface is at a depth of 1414 m, and the computational domain extends 402 m in the x direction, 402 m in the y direction, and 61 m in z (depth). The domain is discretized into $20 \times 20 \times 10$ cells. Boundary conditions for the external grid edges are no-flow and zero displacement. The initial porosity is set at 30% throughout the reservoir. The horizontal permeability varies from 5 to 100 md in depth. Initial fluid saturations for the reservoir are 20% water and 80% oil, with no free gas. The average reservoir pressure is 21.03 MPa initially with bubble point pressure for the fluid set at 20.79 MPa.

ACRES uses an incomplete LU preconditioner (Strang, 1986) with generalized conjugate residual iteration to solve the linear equations for pressure and a direct solver for displacements. ACRES time steps varied from 0.01 to 5 days. IPARS linearizes the coupled set of flow equations via Newton's method and then solves the resulting linear system using a GMRES solver (Axelsson, 1994) with multi-level preconditioner (Edwards, 1998). The GMRES solver had a tolerance of 1×10^{-4}, the Newton solver a tolerance of 1×10^{-6}. Time steps in IPARS ranged in duration from 1 to 10 days.

As expected, the reservoir pressure drops throughout the field because the rate of production exceeds that of injection. The rate of decrease is not uniform, however. A gradient is produced between the two wells. The greatest pressure decrease (and hence porosity decrease and displacements) occurs at the production well, and the least change occurs at the injection well. In this experiment, permeability is held fixed at the initial values throughout the simulation in order to facilitate comparison to ACRES. Fig. 2 shows gas saturation contours from the IPARS/JAS3D simu-
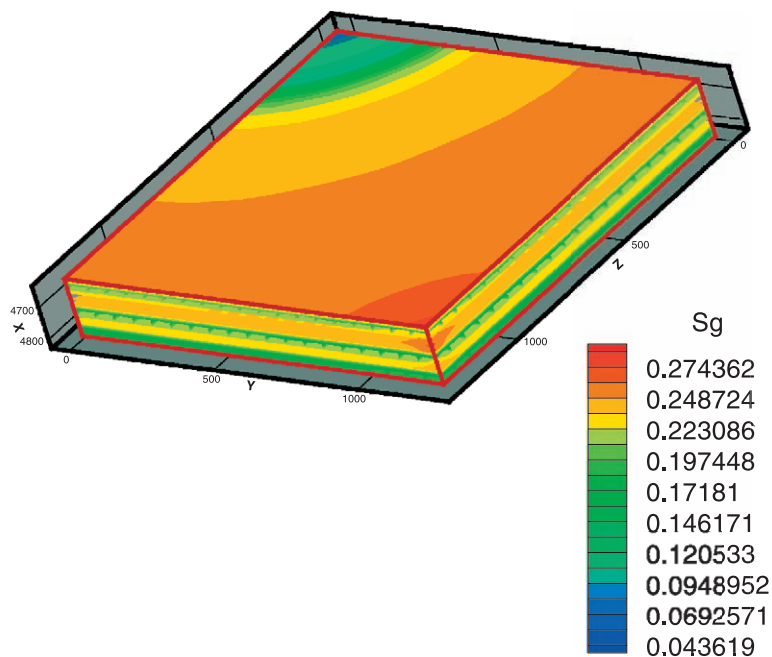

Fig. 2. Contour plot of gas saturation (dimensionless) from IPARS/JAS3D at the end of the 25-year waterflood validation simulation (Numerical Experiment 1). The front corner of the domain contains the production well. The back corner contains the injection well. At the start of simulation, the reservoir contains no free gas. Production causes a drop in pressure and the formation of gas in the reservoir.

lation at 25 years. Initially there is no gas in the field, but as the pore pressure drops below the bubble point pressure during production, gas comes out of solution changing the problem from two- to three-phase flow. At the end of the simulation, the field contains 27% gas near the production well. In a similar fashion, oil pressure contours depicted in Fig. 3 show an overall pressure drop in the field (from initial pressures of 20.68 MPa) with the largest decrease at the production well (where the final pressures are around 4.69 MPa). At the injection well the final pressures are about twice this value 8.96 MPa. Finally, Fig. 4 shows the change in porosity at 25 years. The initial reservoir porosity was homogeneous at 30%. The final porosities show a decrease of almost 13% over the initial simulation porosities (giving values near the production well of less than 26%).

In order to test the sensitivity of the results to the frequency of mechanics steps, a suite of six IPARS/JAS3D simulations was run. The first two experiments took 15- and 30-day mechanics time steps, respectively. As the output was essentially identical between these two simulations, additional runs were performed with 90-day, 1-year, 2-year, and 5-year mechanics time steps. The "critical time step" for

mechanics for this experiment seems to be 2 years. In other words, the simulations with mechanics time steps ranging from 15 days all the way up to 2 years produced the same IPARS/JAS3D displacement histories at the wells. When the mechanics time steps were lengthened to 5 years, however, a noticeable change appeared in the loosely coupled solution.

Fig. 5 compares vertical displacement at the two well locations (producer and injector) for ACRES vs. IPARS/JAS3D. The three black curves correspond to vertical displacement histories at the production well. The three red curves correspond to vertical displacements at the injection well. The dashed red and black curves are the ACRES displacements. The solid red and black curves are the IPARS/JAS3D simulation results for five of the six simulations (JAS3D time steps of 15 days, 30 days, 90 days, 1 year, and 2 years). Finally, the red and black dashed curves with superimposed geometric shapes correspond to the vertical displacement histories resulting from the IPARS/JAS3D simulation with 5-year JAS3D time steps. The dashed (ACRES) and solid (IPARS/JAS3D) lines are qualitatively similar with a quantitative discrepancy of approximately 10% which is most likely due to remaining differences in the ACRES and IPARS flow
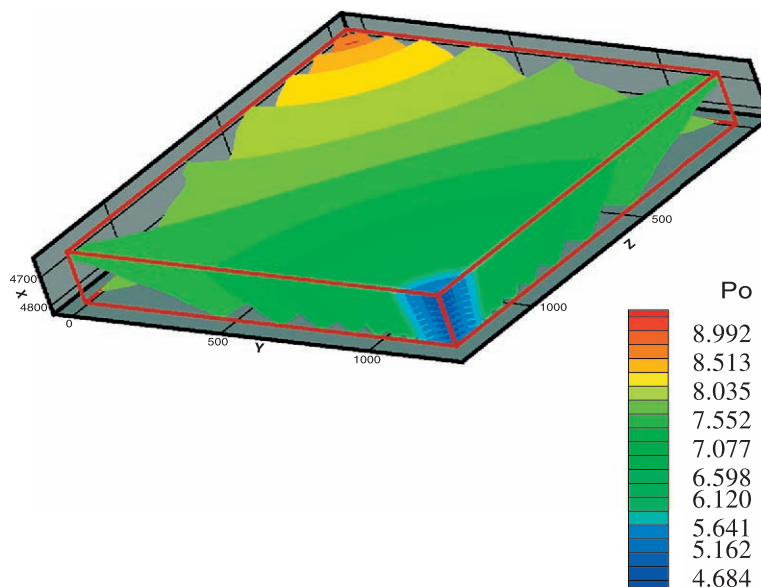

Fig. 3. Contour plot of oil pressure (MPa) from IPARS/JAS3D at the end of the 25-year validation simulation (Experiment 1). The front corner of the domain contains the production well. The back corner contains the injection well. The average reservoir pressure is 21.03 MPa at the start of simulation.
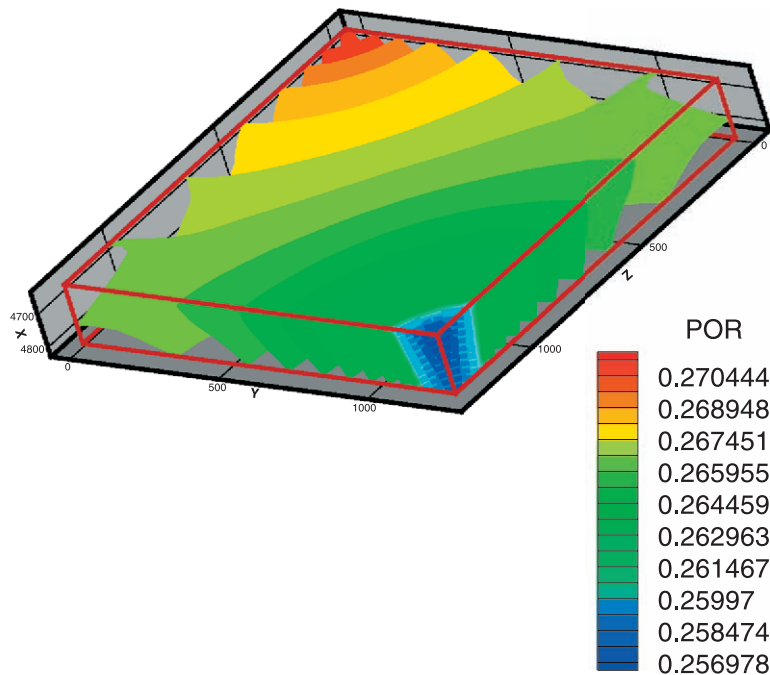
Fig. 4. Contour plot of porosity (dimensionless) from IPARS/JAS3D at the end of the 25-year validation simulation (Experiment 1). The front corner of the domain contains the production well. The back corner contains the injection well. Porosity is uniform at 30% throughout the reservoir at the start of simulation.

solutions. This figure shows that for this 25-year simulation, no difference exists between taking 13 mechanics time steps and taking 600 (every 2 years or every 15 days). This example illustrates the benefits of loose coupling. The simulation captures the fundamental physics at a tiny fraction of the cost of running a fully coupled simulation. When the mechanics time steps are lengthened to every 5 years, however, the loosely coupled simulation results diverge substantially from the fully coupled result. At 10 years (the second mechanics time step), IPARS/JAS3D is able to recover back to the smaller IPARS/JAS3D time step solution (and hence to the fully coupled ACRES solution). More complicated models for mechanics (plastic) might not be so easy to match with such long mechanics time steps in the loosely coupled model and would require further investigation.

7.2. Single layer Belridge experiment

The second example is based on data from the Belridge Field west of Bakersfield, CA. The field was estimated to have more than 500 Mm^3 of original oil-in-place. The field contains two reservoirs: a smaller reservoir located in the shallow Tulare sand, and a slightly deeper reservoir located in diatomite and extending nearly 305 m in depth. Despite the fact that this large diatomite reservoir was discovered in the early 1900s, by the mid-1990s, most of the production was still focused on the Tulare reservoir (Fredrich et al., 1996). The diatomite has unusual geologic properties which make production difficult. This reservoir has very high porosities ranging from 45% to 70%, but very low permeability (~ 0.1 md). In the mid-1970s, hydraulic fracturing allowed production in this field for the first time. With increased production came substantial subsidence, however (up to 6 m at the earth's surface in places), and hence well failures which by the mid-1990s amounted to a well failure rate of 2–5% annually (Fredrich et al., 1996).

Although the reservoir contains multiple sedimentary layers, for simplicity, the synthetic experiment models only one of these layers. This layer (J) is the weakest of the diatomite layers, with an elastic mod-
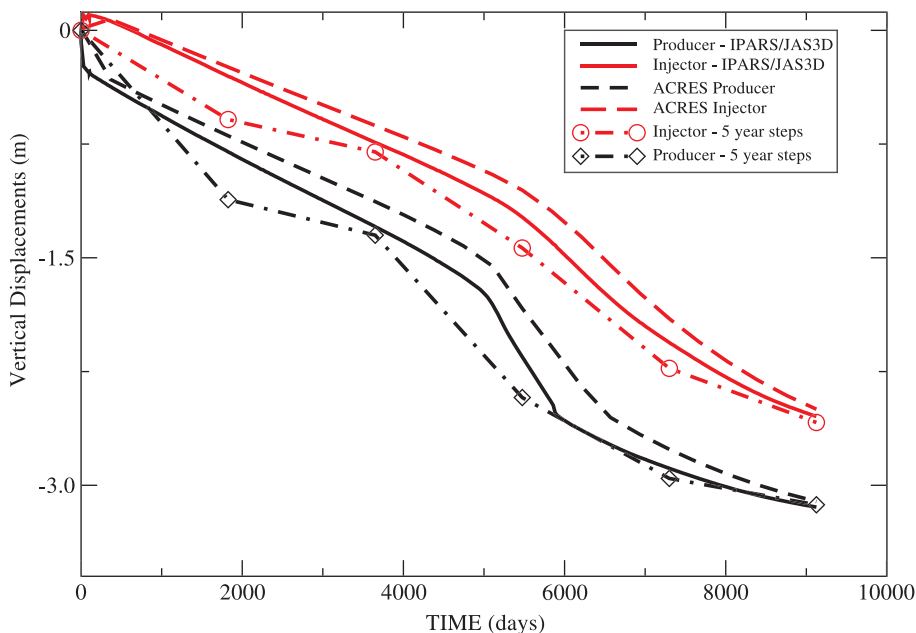
Fig. 5. Comparison of displacement histories at the production and injection wells for the fully coupled ACRES simulator vs. the loosely coupled IPARS/JAS3D simulator. Solid lines: IPARS/JAS3D solution with 15-day JAS3D time steps (same as result for JAS3D time steps up to 2 years). Dashed lines: ACRES solution. Dash-dotted lines with circles/squares: IPARS/JAS3D solution using 5-year JAS3D time steps.

ulus that is $15 \times$ weaker than sandstone (Fossum and Fredrich, 2000).

This example has four production wells in the corners of the rectangular domain, and each well extends to a different depth in the reservoir. The experimental domain was broken into 21 grid blocks in x and in y and 18 blocks in z. The grid spacing was 5 m in x and y, 2.4 m in z. So the reservoir extends a total of 106 m in x and y and 44 m in z. The top of the reservoir is located at a depth of 361 m in the earth

with an initial pore pressure of 3.76 MPa. The initial water saturation is 0.314 with no free gas. The porosity is uniform throughout the domain at 50%. The permeability is isotropic and homogeneous at 0.1 md. The calculation simulated 5 years of coupled flow and mechanics. IPARS took time steps which ranged from 0.2 to 10 days. The JAS3D time steps occurred every 30 days.
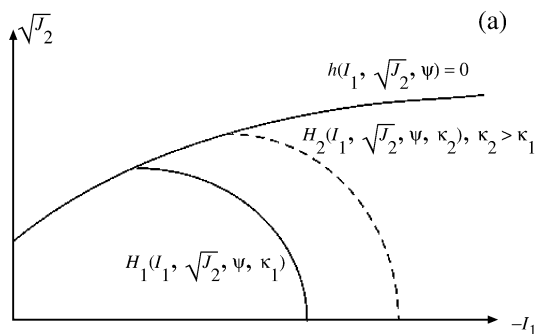

Fig. 6. Yield surfaces for implemented cap/plasticity constitutive model.
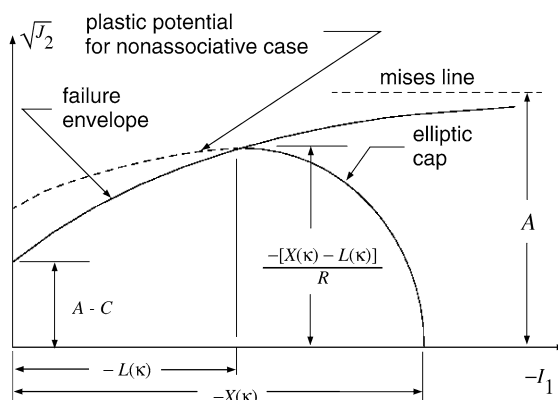

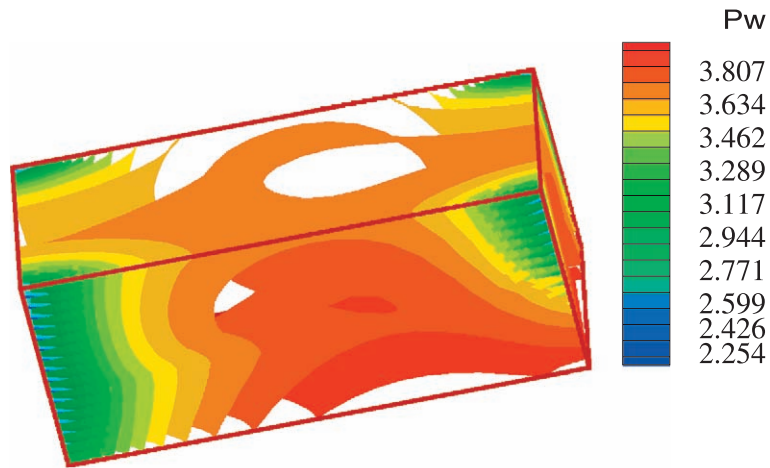Fig. 7. Schematic of modified Sandler–Rubin cap/plasticity constitutive model.

Fig. 8. Water pressure contours (MPa) at the end of a 5-year flow simulation (with no mechanical deformation) for the Belridge Field example (Experiment 2).

The diatomite has a Young's modulus of 413.68 MPa and a Poisson's ratio of 0.2. A modified Sandler–Rubin cap/plasticity constitutive model defines the diatomite behavior. This constitute relation is described in Appendix A and illustrated in Figs. 6 and 7. The material constants have values of $A = 35,333$ MPa, $B = 2.211657 \times 10^{-16}$ Pa^{-1}, and $C = 35,333$ MPa. The parameter K (ratio of yield stress in triaxial extension to triaxial compression) has a value of 0.7953. The ratio of major to minor axes in the cap, R, has value 1.599. Other material parameters include

the maximum plastic volumetric compaction the material can experience under hydrostatic loading, $W = 2335.3$, as well as material constants $D_1 = 1.284887 \times 10^{-16}$ Pa^{-1} and $D_2 = 0.0$ Pa^{-2}. Finally, the initial cap position X_0 is -1.117 MPa. The rock compressibility was estimated for the preconditioner at 4.3512×10^{-9} Pa^{-1}.

Contrasting the results of flow simulation (IPARS) alone on this data with coupled flow simulation and mechanical deformation (IPARS/JAS3D), it is clear that by the end of the 5-year flow simulation, the
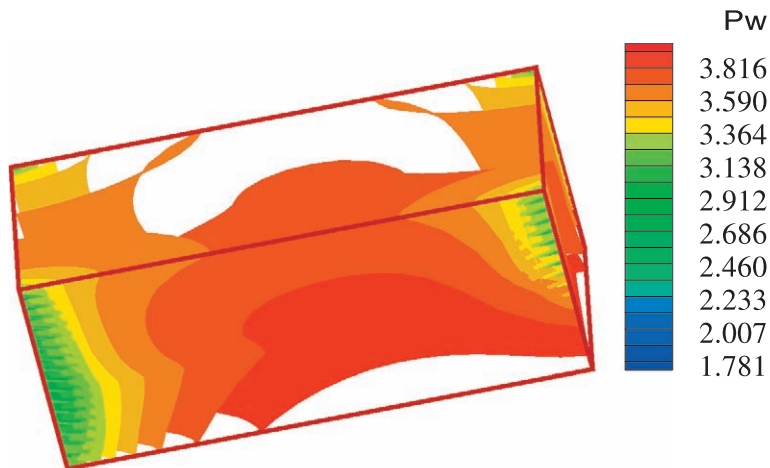

Fig. 9. Water pressure contours (MPa) at the end of 5 years of coupled flow and mechanical deformation modeling. For this Belridge Field experiment (Experiment 2), both porosity and permeability change dynamically with time. Pressures should be compared to those from flow alone (Fig. 8).

MAGNIFIED BY 1.000
ELEMENT BLOCKS ACTIVE:
 1 OF 1

EQTOT
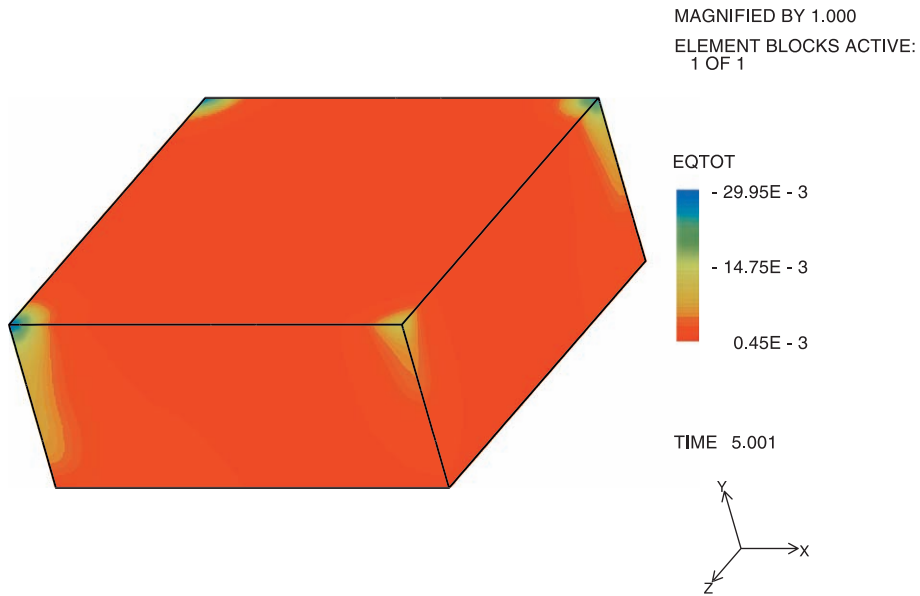
- 29.95E - 3

- 14.75E - 3

0.45E - 3

TIME 5.001

Fig. 10. Equivalent total strain (dimensionless) at the end of the 5-year coupled flow and mechanics simulation of the synthetic Belridge Field data.

pressures have decreased by 40% from their initial values. At the end of the coupled flow and mechanics simulation, the pressures had decreased by 50%. A maximum difference in pressure between the two simulations occurs at the production wells (about 0.45 MPa). Refer to Fig. 8 for the pressures from flow alone and Fig. 9 for the water pressures from coupled flow and mechanics.
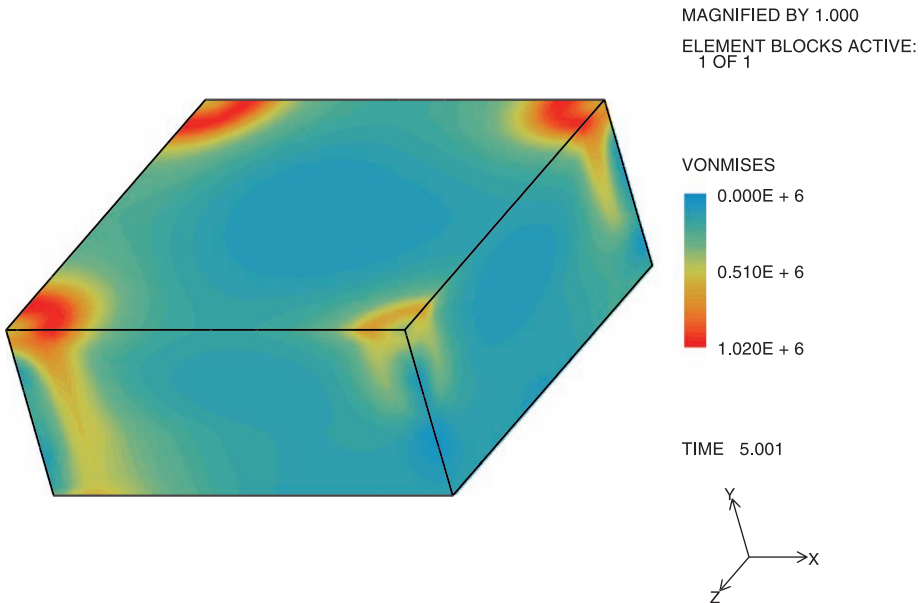
MAGNIFIED BY 1.000
ELEMENT BLOCKS ACTIVE:
 1 OF 1

VONMISES

0.000E + 6

0.510E + 6

1.020E + 6

TIME 5.001

Fig. 11. Vonmises stress (Pa) at the end of the 5-year coupled flow and mechanics simulation of the synthetic Belridge Field data.

MAGNIFIED BY 1.000

ELEMENT BLOCKS ACTIVE:
1 OF 1

DISPLY

- 0.1500
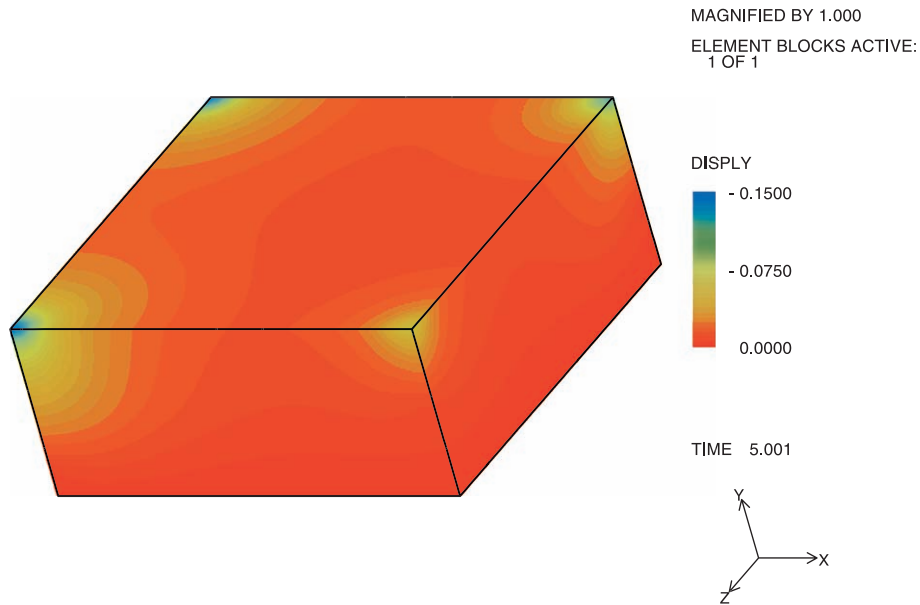
- 0.0750

0.0000

TIME 5.001

Fig. 12. Displacement (m) at the end of the 5-year coupled flow and mechanics simulation of the synthetic Belridge Field data.

Fig. 10 shows equivalent total strain contours at the end of the coupled flow and deformation run. Total strain at the end of the run is 3%. Fig. 11 shows Von Mises stress for the coupled simulation, and one can see the 3-D variations in stress at the wells which is due to different well schedules and different well completion depths. At the end of 5 years of coupled simulation, a maximum subsidence of 0.15 m has occurred at the wells (Fig. 12). During coupled simulation, porosity decreases by 2%, but the permeabilities show the biggest change, decreasing from 0.1 to 0.001 md at the wells. Fig. 13 shows the final permeability at the end of the coupled run.

Feedback occurs when the reservoir parameters change dynamically during flow. Changes in porosity and permeability coming from the mechanics code

Px

0.0934712
0.0837725
0.0740737
0.064375
0.0546762
0.0449775
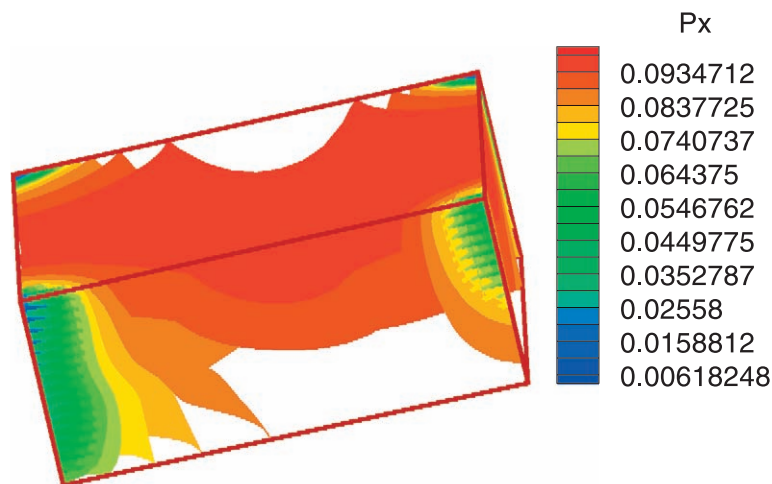0.0352787
0.02558
0.0158812
0.00618248

Fig. 13. Permeability (md) at the end of the 5-year coupled flow and mechanics simulation of synthetic Belridge Field data. At the start of simulation, the permeabilities were 0.1 md uniformly throughout the reservoir.

impact pressures coming out of flow simulator, which in turn impact future parameter changes produced by mechanics. Such nonlinear phenomena are difficult to predict and are often not evident in uncoupled (or simple coupled) models.

8. Conclusions

Defining a fully coupled model for complex multiphase flow and large nonlinear inelastic mechanical deformation is costly and time-consuming. An alternative is to loosely couple two preexisting flow and mechanics simulators. Staggered-in-time coupling and two-way passage of information allow accurate modeling of a range of reservoir conditions. The staggered-in-time loose coupling scheme alternates between flow and mechanics. The mechanics simulator produces updated reservoir parameters which are used by the flow simulator in the next set of time steps. This technique has the advantage that the simulation domains for flow and mechanics can be substantially different (even within the reservoir). There is no need to simulate flow in the non-reservoir rocks as often must be done in full coupling.

The primary bottleneck to this technique is that only relatively small jumps in porosity can be handled due to the large volume of fluids which must move to the wells to conserve mass when compaction occurs in the field. An approximate rock compressibility (used only as a Newton's method preconditioner) helps guide the flow solver toward a solution when both porosity and permeability change substantially with time.

A poroelastic waterflood experiment provides a validation of the loose coupling scheme against a fully coupled simulator from ARCO (ACRES). Good agreement was achieved between ACRES and IPARS/JAS3D at the wells. In fact, a time-step study revealed little difference in the coupled solution when the JAS3D mechanics time steps ranged from 15 days to 2 years. It is considerably cheaper to do a mechanics simulation once every 2 years than every time a flow step is taken (as in full coupling). An adaptive time-stepping strategy for measuring the degree of nonlinearity in the problem and hence optimizing the mechanics time step will maximize the cost-saving benefits of loose coupling.

Nomenclature

B_i	formation volume factor for fluid phase i
c_r	rock compressibility
D	depth
$\mathbf{f}_i$	body force vector
g	gravitational acceleration constant
k_{ri}	relative permeability of phase i
K	absolute permeability
N_i	stock tank volume of component i
P_i	phase pressure
q_i	injection rate for phase i
R_o	stock tank volume of gas dissolved in oil
R_{so}	solution gas ratio
S_i	phase saturation
U_i	fluid phase velocity
$\mathbf{x}_j$	geomechanics position vector
δ_{ij}	Kronecker delta function
Δt	time step
Δx	spatial step in x direction
Δy	step in y direction
Δz	step in z direction
ϵ_v	total volume strain
θ_i	displacement
λ	mobility
μ_i	viscosity
ρ	density
ρ_{is}	stock tank density of component i
σ_{ij}	Cauchy stress tensor
ϕ	porosity
Ω_U	portion of mechanics boundary with kinematic constraints
Ω_T	portion of mechanics boundary with tractions

Appendix A. Plastic-cap constitutive model for geomechanics

JAS3D contains over 50 different constitutive
relationships which can be used to simulate deforma-
tion of a range of materials. The code has been used
extensively to simulate well failure in the Belridge
Field of California. In one of the two numerical
examples in this paper (see Section 7.2), a modified
Sandler–Rubin cap/plasticity constitutive relationship
developed specifically to model compaction of Bel-
ridge diatomite is used. The cap/plasticity model was
developed to allow a more realistic representation of
the mechanical behavior of porous soil or rock than
the basic Drucker–Prager model (one of many con-
stitutive models already in the code). The cap/plasti-
city model is a multi-surface model that generalizes
the Sandler–Rubin constitutive model (Sandler and
Rubin, 1979), incorporating Lode-angle dependence
of yield in the deviatoric plane and nonassociativity in
the meridional plane on the shear failure surface. The
yield surfaces for this model are depicted schemati-
cally in Fig. 6, where the abscissa is $I_1 = \sigma_{kk}$ and the
ordinate is $\sqrt{J_2} = \sqrt{(s_{ij}s_{ij})/2}$, with s_{ij} being the stress
deviator. As seen in the figure, the loading function is
assumed to be isotropic and to consist of two parts: an
ultimate shear failure surface, which serves to limit
the maximum shear stresses attainable by the material,
and an elliptically shaped strain-hardening surface, or
"cap", which produces plastic volume and shear
strains as it moves (say from H_1 to H_2 as depicted
in Fig. 6). The failure envelope portion of the loading
function is:

$$h(I_1, \sqrt{J_2}, \Psi) = \Gamma\sqrt{J_2} - [A - C\exp(BI_1)] = 0$$

where A, B, and C are material constants and Γ is a
function of J_3, the third invariant of the deviator
stress, which incorporates the Lode-angle dependence
of yield as

$$\Gamma = \left\{[1 + \sin(3\Psi)] + [1 - \sin(3\Psi)]/K^*\right\}/2.$$

K^* is the ratio of the yield stress in triaxial
extension to triaxial compression. The Lode angle is

$$\Psi = \frac{1}{3}\arcsin\left(-\frac{27}{2}\frac{J_3}{(3J_2)^{3/2}}\right)$$

for $-\pi/6 \leq \Psi \leq \pi/6$. For triaxial extension, $\Psi = -\pi/6$
and for triaxial compression, $\Psi = \pi/6$. The strain-hard-
ening (cap surface) is of the form:

$$
\begin{aligned}
&H(I_1, \sqrt{J_2}, \Psi, \kappa) \\
&= \Gamma\sqrt{J_2} - \frac{1}{R}\sqrt{[X(\kappa) - L(\kappa)]^2 - [I_1 - L(\kappa)]^2}
\end{aligned}
\tag{A.1}
$$

where R denotes the ratio of the major to minor axes in
the elliptical cap. The cap is chosen so that the tangent
at its intersection with the failure envelope is horizon-
tal. The intersections of the elliptic cap with the I_1 axis
and with the failure envelope are denoted by $-X(\kappa)$
and $-L(\kappa)$, respectively. The hardening parameter κ is
a function of plastic volume strain

$$
\begin{aligned}
\kappa = \epsilon_{kk}^p = W\{&\exp[D_1(X(\kappa) - X_0) \\
&- D_2(X(\kappa) - X_0)^2] - 1\}.
\end{aligned}
\tag{A.2}
$$

In Eq. (A.2), W, D_1, and D_2 are material parame-
ters, with W defining the maximum plastic volumetric
compaction that the material can experience under
hydrostatic loading. The variable X_0 is the initial cap
position. Eqs. (A.1) and (A.2) indicate that the cap is
not fixed in principal stress space, but that it changes
as plastic deformation takes place. In the nonassocia-
tive case, the plastic potential takes the form of an
ellipse as illustrated in Fig. 7. The functional form of
this potential is given by

$$
\begin{aligned}
G(J_1, \sqrt{J_2}, \Psi, \kappa) = \Gamma\sqrt{J_2} &- \frac{[L(\kappa) - X(\kappa)]}{R[X^* - L(\kappa)]} \\
&\times \sqrt{[X^* - L(\kappa)]^2 - [I_1 - L(\kappa)]^2}
\end{aligned}
$$

with $X^* = \ln(A/C)/B$. Parameters in this model can be
found using a procedure described in Fossum et al.
(1995).

References

Arbogast, T., Wheeler, M., Yotov, I., 1996. Logically rectangular mixed methods for flow in heterogeneous domains. In: Aldama, A., et al. (Eds.), Computational Methods in Water Resources XI. Comp. Mech. Publ., Southampton, UK, pp. 621–628.

Arbogast, T., Wheeler, M., Yotov, I., 1997. Mixed finite elements for elliptic problems with tensor coefficients as cell-centered finite differences. SIAM J. Numer. Anal. 34 (2), 828–852.

Arbogast, T., Dawson, C., Keenan, P., Wheeler, M., Yotov, I., 1998a. Enhanced cell-centered finite differences for elliptic equations on general geometry. SIAM J. Sci. Comp. 19 (2), 404–425.

Arbogast, T., Minkoff, S., Keenan, P., 1998b. An operator-based approach to upscaling the pressure equation. In: Burganos, V., Karatzas, G., Payatakes, A., Brebbia, C., Gray, W., Pinder, G. (Eds.), Computational Methods in Water Resources XII. Computational Mechanics Publication, Southampton, UK, pp. 405–412.

Arguello, J., Stone, C., Fossum, A., 1998. Progress on the development of a three-dimensional capability for simulating large-scale complex geologic processes. Proceedings of the 3rd North American Rock Mechanics Symposium. ISRM, Rotterdam. No. USA-327-3.

Axelsson, O., 1994. Iterative Solution Methods. Cambridge Univ. Press, New York.

Biffle, J., 1993. JAC3D—a three-dimensional finite element computer program for the nonlinear quasistatic response of solids with the conjugate gradient method. Technical Report, SAND87-1305, Sandia National Labs, Albuquerque, NM.

Christie, M., 1996. Upscaling for reservoir simulation. J. Pet. Technol. 48, 1004–1010.

Christie, M.A., Mansfield, M., King, P.R., Barker, J.W., Culverwell, I.D., 1995. A renormalisation-based upscaling technique for WAG floods in heterogeneous reservoirs. Proceedings of the 13th Reservoir Simulation Symposium. SPE 29127, pp. 353–361. San Antonio, TX.

Dean, R., Gai, X., Stone, C., Minkoff, S., 2003. A comparison of techniques for coupling porous flow and geomechanics. Proceedings of the 17th Reservoir Simulation Symposium. SPE 79709. Houston, TX.

Durlofsky, L., 1991. Numerical calculation of equivalent grid block permeability tensors for heterogeneous porous media. Water Resour. Res. 27, 699–708.

Durlofsky, L.J., Jones, R.C., Milliken, W.J., 1994. A new method for the scale up of displacement processes in heterogeneous reservoirs. Proceedings of the 4th European Conference on the Mathematics of Oil Recovery. Roros, Norway.

Durlofsky, L.J., Behrens, R.A., Jones, R.C., Bernath, A., 1996. Scale up of heterogeneous three dimensional reservoir descriptions. SPE J. 1, 313–326.

E, W., 1992. Homogenization of scalar conservation laws with oscillatory forcing terms. SIAM J. Appl. Math. 52, 959–972.

Edwards, H.C., 1998. A parallel multilevel-preconditioned GMRES solver for multiphase flow models in the Implicit Parallel Accurate Reservoir Simulator. Texas Institute for Computational and Applied Math Report. University of Texas, Austin, TX.

Espedal, M.S., Saevareid, O., 1994. Upscaling of permeability based on wavelet representation. Proceedings of the 4th European Conference on the Mathematics of Oil Recovery. Roros, Norway.

Fossum, A., Fredrich, J., 2000. Constitutive models for the Etchegoin Sands, Belridge Diatomite, and overburden formations at the Lost Hills Oil Field, California. Technical Report, SAND2000-0827, Sandia National Labs, Albuquerque, NM.

Fossum, A., Senseny, P., Pfeifle, T., Mellegard, K., 1995. Experimental determination of probability distributions for parameters of a salem limestone cap plasticity model. Mech. Mater. 21, 119–137.

Fredrich, J., Arguello, J., Thorne, B., Wawersik, W., Deitrick, G., de Rouffignac, E., Myer, L., Bruno, M., 1996. Three-dimensional geomechanical simulation of reservoir compaction and implications for well failures in the Belridge Diatomite. Proceedings of the SPE Annual Technical Conference and Exhibition, No. 36698. SPE, Richardson, TX, pp. 195–210.

Fredrich, J., Deitrick, G., Arguello, J., de Rouffignac, E., 1998. Reservoir compaction, surface subsidence, and casing damage: a geomechanics approach to mitigation and reservoir management. Proceeding of SPE/ISRM EUROCK 1998, No. 47284. SPE and ISRM.

Fung, L.-K., Buchanan, L., Wan, R.G., 1994. Coupled geomechanical–thermal simulation for deforming heavy-oil reservoirs. J. Can. Pet. Technol. 33 (4), 22–28.

Hou, T.Y., Wu, X.H., 1997. A multiscale finite element method for elliptic problems in composite materials and porous media. J. Comput. Phys. 134, 169–189.

King, P.R., Muggeridge, A.H., Price, W.G., 1993. Renormalization calculations of immiscible flow. Transp. Porous Media 12, 237–260.

King, M.J., King, P.R., McGill, C.A., Williams, J.K., 1995. Effective properties for flow calculations. Transp. Porous Media 20, 169–196.

Lake, L.W., 1989. Enhanced Oil Recovery. Prentice-Hall, Englewood Cliffs, NJ.

Lewis, R., Ghafouri, H., 1997. A novel finite element double porosity model for multiphase flow through deformable fractured porous media. Int. J. Numer. Anal. Methods Geomech. 21, 789–816.

Lewis, R., Sukirman, Y., 1993a. Finite element modelling for simulating the surface subsidence above a compacting hydrocarbon reservoir. Int. J. Numer. Anal. Methods Geomech. 18, 619–639.

Lewis, R., Sukirman, Y., 1993b. Finite element modelling of three-phase flow in deforming saturated oil reservoirs. Int. J. Numer. Anal. Methods Geomech. 17, 577–598.

Lu, Q., 2000. A parallel multi-block/multi-physics approach for multi-phase flow in porous media. PhD thesis, University of Texas at Austin, Austin, TX.

Lu, Q., Peszynska, M., Wheeler, M.F., 2001. A parallel multi-block black-oil model in multi-model implementation. Proceedings of the 16th Reservoir Simulation Symposium, No. 66359. SPE, Richardson, TX.

Minkoff, S., Stone, C., Arguello, J., Bryant, S., Eaton, J., Peszynska, M., Wheeler, M., 1999. Coupled geomechanics and flow simulation for time-lapse seismic modeling. Proceedings of the 69th Annual International Meeting. SEG, Tulsa, OK, pp. 1667–1670.

Osorio, J., Chen, H., Teufel, L., 1999. Numerical simulation of the impact of flow-induced geomechanical response on the productivity of stress-sensitive reservoirs. Proceedings of the 15th Reservoir Simulation Symposium, No. 51929. SPE, Richardson, TX, pp. 373–387.

Parashar, M., Pope, G., Wang, K., Wang, P., Wheeler, J., 1997. A new generation EOS compositional reservoir simulator: Part II. Framework and multiprocessing. Proceedings of the 14th Reservoir Simulation Symposium, No. 37977. SPE, Richardson, TX.

Peaceman, D., 1977. Fundamentals of Numerical Reservoir Simulation. Elsevier, New York.

Peaceman, D., 1983. Interpretation of well-block pressure in numerical reservoir simulation with non-square grid blocks and anisotropic permeability. SPE J. 23 (3), 531–543.

Peszynska, M., Lu, Q., Wheeler, M.F., 1999. Coupling different numerical algorithms for two phase fluid flow. In: Whiteman, J.R. (Ed.), Proceedings of Mathematics of Finite Elements and Applications. Brunel University, Uxbridge, UK, pp. 205–214.

Peszynska, M., Wheeler, M., Yotov, I., 2002. Mortar upscaling for multiphase flow in porous media. Comput. Geosci. 6 (1), 73–100.

Russell, T., Wheeler, M., 1983. Finite element and finite difference methods for continuous flows in porous media. In: Ewing, R.E. (Ed.), The Mathematics of Reservoir Simulation. SIAM, Philadelphia, pp. 35–106.

Sandler, I., Rubin, D., 1979. An algorithm and a modular routine for the cap model. Int. J. Numer. Anal. Methods Geomech. 3, 173–186.

Settari, A., Mourits, F., 1994. Coupling of geomechanics and reservoir simulation models. In: Siriwardane, Zaman (Eds.), Computer Methods and Advances in Geomechanics. Balkema, Rotterdam, pp. 2151–2158.

Settari, A., Walters, D., 1999. Advances in coupled geomechanical and reservoir modeling with applications to reservoir compaction. Proceedings of the 15th Reservoir Simulation Symposium, No. 51927. SPE, Richardson, TX, pp. 345–357.

Stone, C., 1997. SANTOS—a two-dimensional finite element program for the quasistatic, large deformation, inelastic response of solids. Technical Report, SAND90-0543, Sandia National Labs, Albuquerque, NM.

Strang, G., 1986. Introduction to Applied Mathematics. Wellesley-Cambridge Press, Wellesley, MA.

Wang, P., Yotov, I., Wheeler, M., Arbogast, T., Dawson, C., Parashar, M., Sepehrnoori, K., 1997. A new generation EOS compositional reservoir simulator: Part I. Formulation and discretization. Proceedings of the 14th Reservoir Simulation Symposium, No. 37979. SPE, Richardson, TX.

Wellman, G.W., 1999. MAPVAR—a computer program to transfer solution data between finite element meshes. Technical Report, SAND99-0466, Sandia National Labs, Albuquerque, NM.

Wheeler, M., Arbogast, T., Bryant, S., Eaton, J., Lu, Q., Peszynska, M., Yotov, I., 1999. A parallel multiblock/multidomain approach for reservoir simulation. Proceedings of the 15th Reservoir Simulation Symposium, No. 51884. SPE, Richardson, TX, pp. 51–61.

Wheeler, M., Wheeler, J., Peszynska, M., 2000. A distributed computing portal for coupling multi-physics and multiple domains in porous media. In: Bentley, L., Sykes, J., Brebbia, C., Gray, W., Pinder, G. (Eds.), Computational Methods in Water Resources. A.A. Balkema, Southampton, UK, pp. 167–174.

Yotov, I., 1998. Mortar mixed finite element methods on irregular multiblock domains. In: Wang, J., et al. (Eds.), Iterative Methods in Scientific Computation, vol. 4. IMACS, Amsterdam, pp. 239–244.